Geometrical and electrical percolation in nanometre-sized Co-cluster assemblies

1999 J. Phys.: Condens. Matter 11 3247

(http://iopscience.iop.org/0953-8984/11/16/006)

J. Phys.: Condens. Matter **11** (1999) 3247–3257. Printed in the UK PII: S0953-8984(99)98294-2

Geometrical and electrical percolation in nanometre-sized Co-cluster assemblies

S Yamamuro†‡§, K Sumiyama†, T Hihara†‡ and K Suzuki†

† Institute for Materials Research, Tohoku University, Sendai 980-8577, Japan
‡ Core Research for Evolutional Science and Technology (CREST) of Japan Science and Technology (JST) Corporation, Honchou 4-1-8, Kawaguchi, Saitama 332-0012, Japan

Received 11 October 1998, in final form 26 January 1999

Abstract. We deposited monodispersed Co-clusters in the size range of 6–13 nm on substrates using the plasma-gas-condensation cluster deposition system. The assembling process of the clusters from discontinuous to continuous networks was investigated by transmission electron microscopy (TEM) and *in situ* electrical conductivity measurement, and discussed in terms of the two-dimensional (2D) percolation concept. The electrical conductivity measurement indicates that the percolation process of Co clusters does not agree with a simple scaling-law: the critical conductivity exponent increases with increasing mean cluster diameter, d, although it is predicted to be independent of d in the ordinary 2D percolation theory. This anomaly is interpreted by the soft-percolation model, implying that there is distribution of electrical contacts between the clusters. The critical coverage of clusters (0.63) is much higher than the predicted one (0.45) irrespective of d, due mainly to the partial overlapping of deposited clusters, and partly to an attractive interaction between the clusters. Such cluster-overlapping also increases the critical thickness of electrical percolation with increasing d.

1. Introduction

Nanometre-scale geometrical and chemical controls of substances are promising to obtain excellent functional materials, i.e. soft-magnetic nanocrystalline materials with a high magnetic flux density, magnetic granular materials with giant magnetoresistance [1, 2], etc. These materials have been usually obtained by precipitation from supersaturated solid solution initially produced by vapour-, liquid- or solid-quenching, in which nanometre-sized particles randomly nucleate and grow from matrices or on substrates. In these processes, the particle size depends on the annealing or deposition time and correlates with the inter-cluster distance because the nucleation and growth of particles are ensured by consumption of solute atoms or adatoms near the growing particles. Thus, a finer-scale structure control in a nanometre order is difficult using these metallurgical processes. These difficulties will be overcome by a direct assembling of nanometre-sized clusters as building blocks.

Moreover, it is well known that nanometre-sized free clusters exhibit unique structures and anomalous properties [3, 4], strongly depending on their size. If we can deposit or arrange these clusters on a substrate with their initial size, structure and properties kept, we can design and fabricate ideally nanostructure-controlled materials. For the material fabrication, we have to improve the efficiency of a cluster source to obtain an intensive cluster beam. We also need to produce monodispersed clusters and control their size precisely. Recently, we have

§ E-mail address: yamamuro@snap8.imr.tohoku.ac.jp.

0953-8984/99/163247+11$19.50

constructed plasma-gas-condensation-type (PGC) cluster-deposition equipment [5–7] based upon both plasma-glow-discharge vaporization and inert gas condensation techniques [8], and succeeded in producing a large number of transition metal clusters whose size is controllable between 6 and 13 nm in diameter with the standard deviation less than 10% of the mean cluster size. Then, we tried to deposit nanometre-sized Co clusters on substrates for cluster-assembling, and observed how these clusters form continuous networks [9].

Such a cluster deposition process can be understood by the percolation concept which is commonly applied to phase transition phenomena in condensed matter [10, 11]. In this concept, a statistical fluctuation arises from occupying or bonding of neighbouring sites by characteristic species or interactions. When the fluctuation is increased, the site-occupied or bond-connected network spreads over an infinite range at the percolation threshold, i.e. the system meets the phase transition. In a real system, a monstrous network becomes predominant and spreads over ultimate boundaries. There have been many experimental reports on the percolation phenomena: the thin-film growth process from discontinuous to continuous states [12], the metal/insulator transition in cermet films [13] and the divergence of electrical conductivity and dielectric constant in the sintered composites consisting of micrometre-sized powders [14]. In addition, it is important to understand the assembling process of deposited clusters in order to obtain well controlled cluster assemblies. Random deposition of clusters is a simple stochastic event, however, the qualitative studies have been reported only for the percolation features of Sb cluster deposition [15, 16].

In this paper, we describe the experimental results of transmission electron microscopy (TEM), *in situ* electrical conductivity measurement during the deposition of monodispersed Co-clusters on substrates, and quantitatively discuss these results in terms of the two-dimensional (2D) percolation concepts.

2. Experimental procedures

Figure 1 shows the PGC-type cluster deposition system, which mainly consists of a sputtering chamber, a growth region and a deposition chamber [6, 7]. In the sputtering chamber, two Co-targets with 70 mm in diameter were sputtered with a facing-target-type dc mode at inert gas (pure Ar gas or Ar/He gas mixture) pressure of about 180 Pa, which is much higher than that in the conventional sputtering. Such high pressure is effective to increase the cluster formation probability. The input power for sputtering was 400 W. A large amount of inert gas was injected steadily into the sputtering chamber, and evacuated by a mechanical booster pump through a small nozzle. Vaporized atoms were carried by a gas flow toward the growth region consisting of a copper tube, which was cooled by liquid nitrogen. The clusters formed in the growth region were ejected through the small nozzle and the two skimmers by differential pumping, and then deposited onto substrates fixed on the sample holder in the deposition chamber whose pressure was about 1×10^{-2} Pa. The substrate temperature was about 300 K during the deposition.

We controlled the mean diameter of Co clusters, d, between 6 and 13 nm by adjusting the Ar gas flow rate, V_{Ar}, and He gas flow rate, V_{He} [17]. TEM observation of Co clusters indicates that the mean cluster size decreases from 13 to 8.5 nm on decreasing V_{Ar} from 8.3×10^{-6} to 5.0×10^{-6} m^3 s^{-1} (from 500 to 300 SCCM). However, it was difficult to produce smaller clusters because the deposition rate rapidly decreased with decreasing V_{Ar}. In order to overcome this problem, He gas was mixed with Ar gas: for example, the cluster size further decreases to 6 nm by mixing He gas ($V_{He} = 9.2 \times 10^{-6}$ m^3 s^{-1} (550 SCCM)) with Ar gas ($V_{Ar} = 4.2 \times 10^{-6}$ m^3 s^{-1} (250 SCCM)). In these samples, the standard deviations are less than 10% of the mean cluster sizes, showing good monodispersiveness. Since He gas has the high

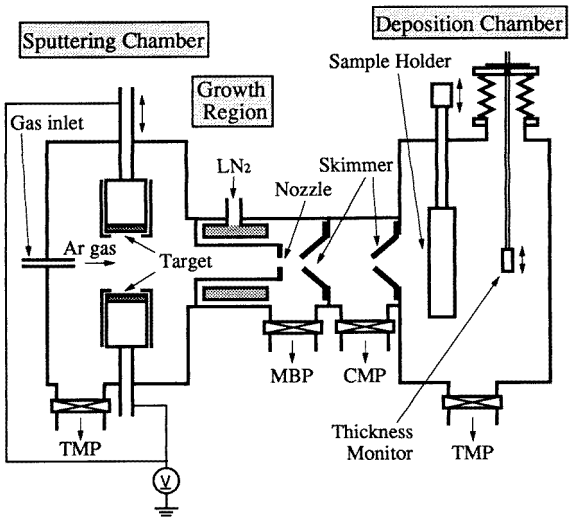

Figure 1. Schematic diagram of the plasma-gas-condensation-type cluster deposition system. TMP, MBP and CMP represent turbo-molecular pump, mechanical booster pump and compound molecular pump, respectively.

thermal conductivity in comparison with Ar gas, it can cool the sputtered metal atoms more effectively in the liquid-nitrogen-cooled growth region. This increases the supersaturation ratio of sputtered atoms, promoting the nucleation and growth processes of clusters. As a whole, mixing of He gas leads to the remarkable increase in the deposition rate.

We used two kinds of substrate for Co-cluster deposition: TEM microgrids for TEM observation, and polyimide films for *in situ* electrical conductivity measurement. The effective film thickness of deposited clusters, t, was estimated using a crystal quartz thickness monitor, which measured the weight of the deposited clusters. Since the present cluster source was very stable during the operation, the proportionality between t and the deposition time was ensured; thus we plot the observed physical quantities as a function of t instead of the deposition time hereafter. We observed deposited Co-clusters using a 200 kV transmission electron microscope (Hitachi HF-2000), and took TEM images as digitized data with a slow-scan CCD camera installed in the electron microscope. The size and connectivity of Co-cluster assemblies were estimated using image-analysis software (Image-Pro PLUS: Media Cybanetics Co). We did *in situ* measurement of electrical conductivity during the deposition by a pseudo-four-probe method. Two electrodes with about 4 mm width and 1 mm separation were predeposited on a polyimide film substrate. The electrical current of 15 μA was applied from a current generator between the two electrodes. Using a constant current mode, the voltage-change between two electrodes was detected with a digital volt meter as a function of the deposition time.

3. Results

Figures 2(a)–(c) show the bright-field TEM images of Co clusters deposited on TEM microgrids as a function of t for the three sizes, $d = 6$, 8.5 and 13 nm, respectively. At $t = 1$ nm, clusters are roughly isolated and some clusters contact each other. With increasing t, the clusters aggregate further form networks, where a partial overlapping of clusters is often observed. However, the individual clusters reveal no marked change in their initial sizes during the

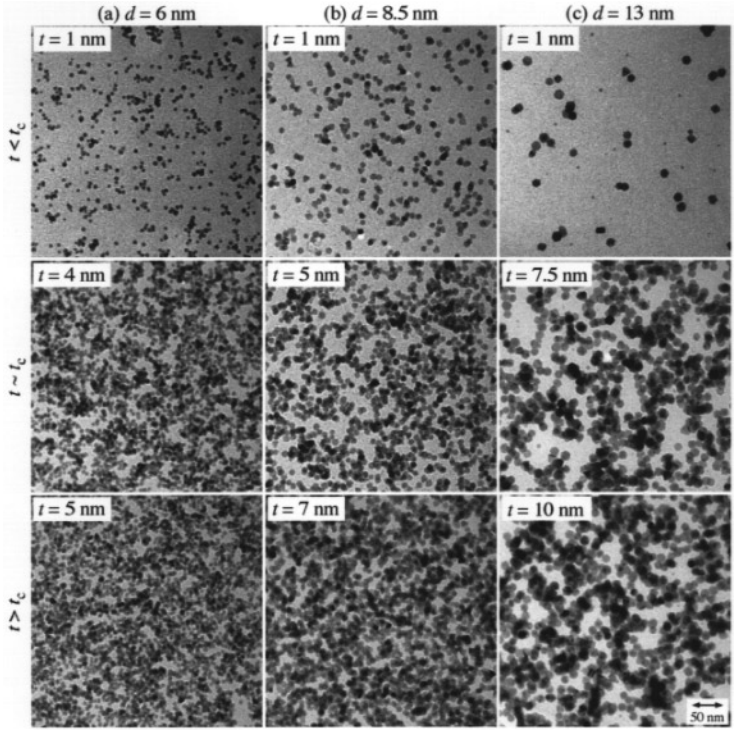

Figure 2. Transmission electron microscope (TEM) images of Co clusters on TEM microgrids as a function of the average deposition thickness of the clusters, t. (a) The mean cluster diameter, $d = 6$ nm, (b) $d = 8.5$ nm and (c) $d = 13$ nm.

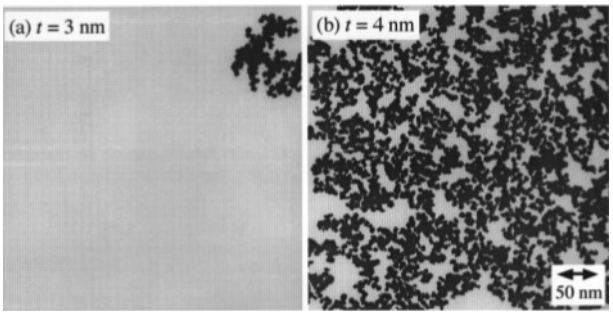

Figure 3. Digitized TEM images of maximum Co-cluster-network for the mean cluster diameter, $d = 6$ nm: (a) The average deposition thickness, $t = 3$ nm and (b) $t = 4$ nm.

deposition. The electron diffraction measurements of these Co-cluster assemblies indicate [17] that the only fcc-rings are observed for $d = 6$ nm, while the hcp-rings slightly appear for $d = 8.5$ nm. The hcp-rings become more marked for $d = 13$ nm, even though the fcc-ones are still predominantly detectable. These results indicate that the Co clusters with the size between 8.5 and 13 nm have fcc and hcp mixed structures or contain a lot of stacking faults.

In order to visualize the geometrical percolation of the Co-cluster assemblies, we minutely examined the connectivity of deposited clusters by analysing the TEM images

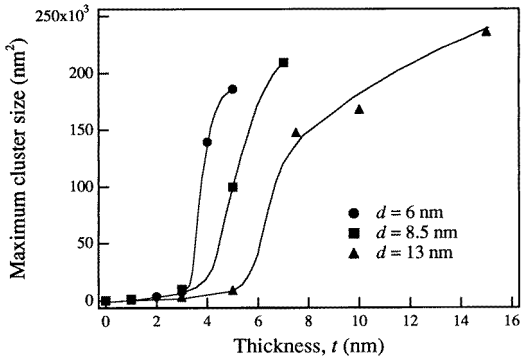

Figure 4. Areal size of maximum Co-cluster-network estimated by TEM for the mean cluster diameters, $d = 6$, 8.5 and 13 nm as a function of the average deposition thickness, t.

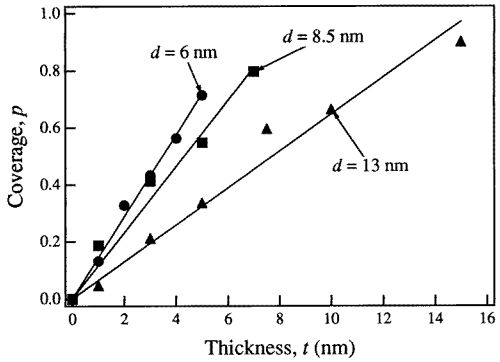

Figure 5. The fraction of cluster-covered area, p, as a function of the average deposition thickness, t, estimated by TEM for the mean cluster diameter, $d = 6$, 8.5 and 13 nm.

using image-analysis software. Figure 3 shows the largest cluster-network picked up from the observed TEM images at typical t values (below/near the percolation threshold) for $d = 6$ nm. In this figure, the apparent size of the largest cluster-network is about 80 nm in a one-dimensional scale at $t = 3$ nm, while it becomes comparable to or larger than the observed area of about 350 nm at $t = 4$ nm. This indicates that the geometrical percolation occurs at $t \sim 4$ nm for $d = 6$ nm. Figure 4 shows the apparent size of the largest cluster-network for $d = 6$, 8.5 and 13 nm as a function of t. It rapidly increases at around the critical thickness of geometrical percolation, $t_{CG} = 3.5 \pm 0.5$, 4.0 ± 1.0 and 6.0 ± 1.0 nm for $d = 6$, 8.5 and 13 nm, respectively.

The correlation between t and a cluster-coverage, p, was also evaluated as shown in figure 5. The p-value linearly increases with t for all of the sizes, suggesting that the deposited Co-clusters cover the substrate surface two dimensionally. The slope of p versus t decreases with increasing d: the slopes are 0.14, 0.12 and 0.07 nm^{-1} for $d = 6$, 8.5 and 13 nm, respectively. This indicates that a smaller cluster deposition is more effective to obtain a continuous cluster assembly.

Figure 6(a) shows the electrical conductivity, σ, for Co-cluster assemblies deposited on polyimide film substrates at ambient temperature (about 300 K) as a function of t. In the initial deposition stage, σ is almost zero because the circuit between the electrodes is opened: the

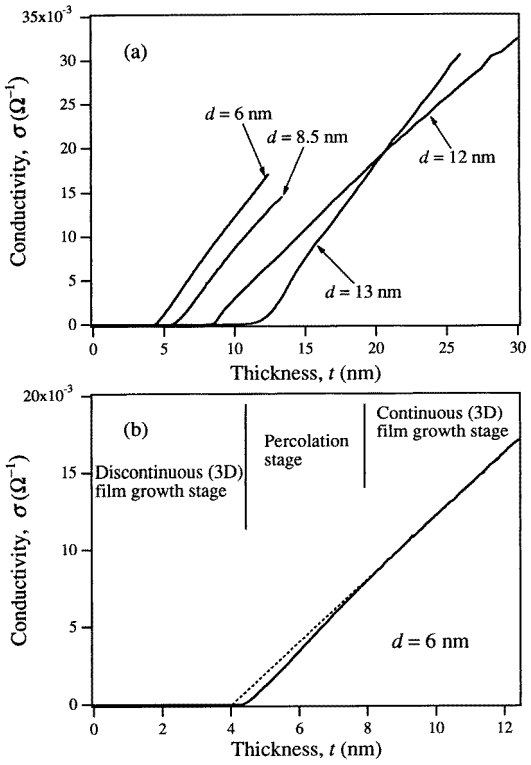

Figure 6. (a) Electrical conductivity, σ, versus the average deposition thickness, t, during the assembling process of Co clusters on polyimide film substrates for the mean cluster diameter, $d = 6$, 8.5, 12 and 13 nm. (b) Enlarged figure of σ versus t for $d = 6$ nm. The broken line in figure 6(a) is extrapolated from the data for $t > 8$ nm.

discontinuous 2D film growth stage. For the specimen with $d = 6$ nm (see figure 6(b)), for example, σ starts to increase rapidly at $t \sim 4$ nm due to the onset of the formation of continuous networks between the electrodes. At $t = 8$ nm, σ versus t shows a slight bend, and then increases linearly with t for $t > 8$ nm: the continuous 3D film growth stage. At $t = 4$–8 nm, the deviation from the straight broken line, extrapolated from the data for $t > 8$ nm, is detectable. Such deviation is also observed for all of the specimens, corresponding to the percolation stage where the number of conduction paths increases dramatically. It is worthwhile to note that the critical thickness where σ starts to increase reveals a peculiar d-dependence: it becomes larger with increasing d.

Using the sliding least-squares fit procedure [12], we fitted the following scaling-law to the measured data of σ near the percolation threshold:

$$\sigma \propto (t - t_{CE})^{\mu} \tag{1}$$

where the critical thickness, t_{CE}, estimated by the electrical conductivity measurement and the critical exponent, μ, are the fitting parameters. We divided the data into 3 nm segments starting at the specific thickness, t_S, and fitted equation (1) to these segments. The detailed fitting results are shown in figure 7(a) for $d = 6$ nm as an example. In this figure, the square of the correlation coefficient, $\rho^2 \cong 1$ for $t_S = 4.4$–6.3, however, $\mu < 1$ at $t_S > 4.8$. Since μ is considered to be larger than 1, the least-squares fit was performed on the data for $t_S = 4.4$–4.8, resulting in $\mu = 1.1$ and $t_{CE} = 4.4$. The log–log plot of σ versus $(t - t_{CE})$ reveals a good linear

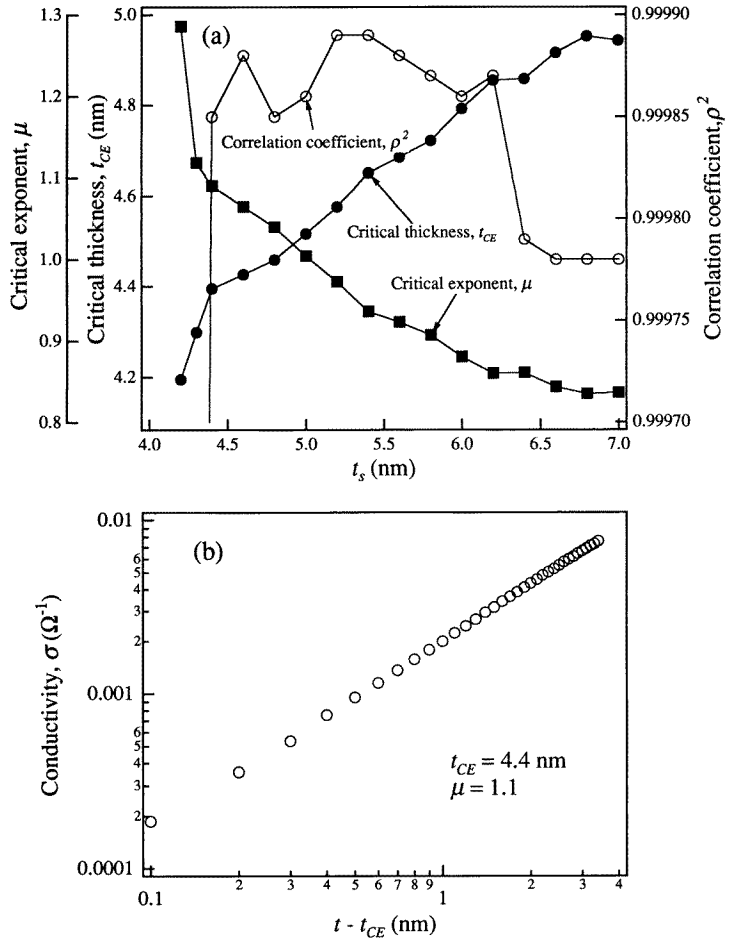

Figure 7. (a) Typical fitting results of the critical thickness, t_{CE}, critical exponent, μ, and square of correlation coefficient, ρ^2, of electrical percolation for Co clusters with $d = 6$ nm as a function of the starting thickness, t_S. These parameters were obtained by fitting equation (1) to the electrical conductivity data using the sliding least-squares fitting procedure. (b) The log–log plot of σ versus $(t - t_{CE})$ for Co clusters with $d = 6$ nm, using the fitting result of $t_{CE} = 4.4$ nm.

correlation (see figure 7(b)), indicating that the fitting is satisfactory in this range. Using the same procedure, we estimated t_{CE} and μ for other specimens and plot them as a function of d in figures 8(a) and (b). As shown in these figures, both t_{CE} and μ exhibit distinct size-dependence, monotonically increasing with d.

The 2D percolation phenomenon is essentially expressed as a function of p. Thus, we convert t into p, using the linear relation between p and t shown in figure 5. Figure 8(c) shows the critical coverage, p_C, estimated from the electrical conductivity as a function of d, indicating that p_C is about 0.63 irrespective of d. This value is much larger than the theoretical one, which is estimated to be about 0.45 in the ordinary 2D lattice percolation systems [18]. Such a large p_C-value has been expected for the 2D continuum percolation of overlapped circles ($p_C = 0.68$) [19]. Indeed, overlapping of deposited clusters were often observed by TEM in the present experiments. A strong attractive inter-cluster interaction also increases the

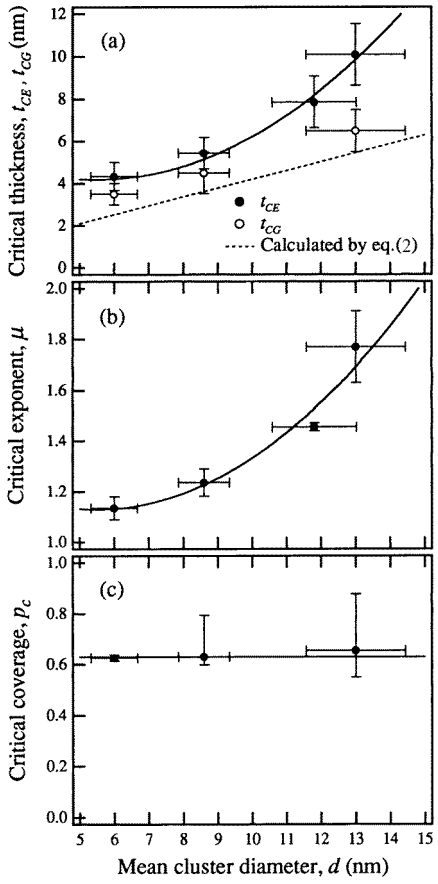

Figure 8. (a) The critical thicknesses of geometrical and electrical percolation, t_{CG} and t_{CE}, (b) critical exponent, μ, and (c) critical coverage, p_C, as a function of the mean cluster diameter, d, for Co-cluster assemblies. The broken line in figure 8(a) indicates the one obtained by equation (2). The solid curves and line in figures 8(a)–(c) give a guide to the eyes and the line in figure 8(c) shows that $p_C = 0.63$.

p_C-value [20], because it promotes inhomogeneous aggregation of clusters. Since the spatial distribution of clusters is not perfectly random in the present case (see figure 2), Co clusters are partially aggregated probably due to magnetic interactions between ferromagnetic Co clusters.

The μ-value is not influenced by the t–p-conversion as long as we use the linear relation between t and p. Thus, it must be noted that μ increases from 1.1 to 1.8 with increasing d from 6 to 13 nm (see figure 8(b)) because the parameters, μ and p_C, depend only on a spatial dimensionality in the ordinary percolation phenomena [10, 11]: they are universal constants. The universality has been extensively confirmed in various percolation systems such as an ordinary lattice percolation [21], thin film formation [12, 22] and metal/insulator composites [13]. Although the μ value of 1.8 for $d = 13$ nm is close to that of 3D percolation ($\sim$1.9) [21], we have confirmed that the 2D growth of the deposited clusters is maintained irrespective of d in the TEM observations. Thus, these results demonstrate that the universality is broken in the present Co-cluster assemblies. Such a nonuniversal conductivity exponent has been theoretically proposed for a random register network [23–28], and hopping or tunnelling

conduction systems [29–31]. It was also observed experimentally in simple composites consisting of conducting and insulating constituents [13, 31, 32], depending only on their concentration. Therefore, the present results give a new size-dependent nonuniversality in the conductivity percolation of the cluster-assembled films.

4. Discussion

Since the percolation phenomena during the cluster-assembling process were detected as a function of t in the present experiments, we first discuss the critical thicknesses, t_{CG} and t_{CE}. The t_{CG}-values are slightly smaller than the t_{CE}-values as shown in figure 8(a). This discrepancy is partly ascribed to the fact that the area observed by TEM is much smaller than that measured by the electrical conductivity: the largest cluster-network observed by TEM is still smaller than the infinite one for discussing the percolation. The quantum percolation theory predicts that the electrical percolation is suppressed by a localization effect, while it is more suppressed in a tunnelling conduction system [11]. However, since the electrical conductivity was measured at room temperature, we cannot discuss such quantum effects in detail.

We then try to interpret the characteristic d-dependence of t_{CE} through the comparison with the result of Sb_n cluster deposition (n is the number of atoms per cluster) [15, 16], where t_{CE} decreases with increasing cluster size: $t_{CE} = 37$ nm for $n = 4$, while $t_{CE} = 2.2$ nm for $n = 1850$. This result contradicts the present results. The discrepancy between Sb and Co cluster assemblies is ascribed to their different mobility and coalescence features on the substrate. Since small Sb clusters easily migrate on a substrate just like adatoms, they coalesce each other at the preferred nucleation sites and further grow by capturing the smaller clusters to form isolated large islands by 3D growth due to the low melting point of Sb. On the other hand, large Sb clusters do not migrate on a substrate because they are anchored to their impinging places. Hence, the continuous Sb film formation is promoted with increasing d, leading to the decrease in t_{CE}. The present Co clusters will hardly migrate on the substrate and exhibit 2D growth without severe coalescence, because they include more than 10^4 atoms and the melting point of Co is much higher than that of Sb. Assuming that the Co cluster is a sphere with the diameter d and randomly placed on a substrate without overlapping, we expect a linear increase in the critical thickness, t_{CE}, with d as follows:

$$t_{CE} = \frac{N(4\pi/3)(d/2)^3}{A} = \frac{p_C A}{\pi(d/2)^2}\frac{4\pi(d/2)^3}{3}\frac{1}{A} = \frac{2p_C}{3}d \qquad (2)$$

where A is the deposited area and N the number of clusters within A. In figure 8(a), the broken line corresponding to equation (2) with $p_C = 0.63$ is much lower than the observed t_{CE} values. The linear d-dependence of t_{CE} in equation (2) is also inappropriate for the nonlinear variation of the experimental t_{CE}-values with d. In the present specimens, however, overlapping of deposited clusters are often observed as mentioned in figure 2. Therefore, the anomalous features in t_{CE} in the present Co-cluster assemblies can be understood by considering the partial overlapping of clusters. The cluster-overlapping also influences the relation between t and p. If the overlapping could be negligible, the data in figure 5 must obey the relation in equation (2) with the indices CE and C left out: $t = (2d/3)p$ or $p = (3/2d)t$. However, the experimental values of the slope of p versus t are about 40% smaller than the expected ones in equation (2): $3/2d = 0.25$, 0.18 and 0.12 nm^{-1} for $d = 6$, 8.5 and 13 nm, respectively.

Finally, we discuss an interpretation for the nonuniversal behaviour of μ. In the present experiments, the deposited clusters occupy the random sites on a substrate and connect with

adjacent clusters in irregular directions. Thus, the 2D continuum percolation model, where circles of equal radius are randomly placed with partial overlapping, is the most appropriate for explaining the present experimental situation. Based on this context, we introduce the soft-percolation model [29, 30], where the occupation sites and/or the bonding strength of clusters are randomly distributed, in contrast to the periodic lattice sites or the unique bonding strength in ordinary 2D percolation systems. In this model, the inter-particle hopping or tunnelling conduction leads to a dynamic percolation process in the spatially disordered system. The important assumption is that the strength of connection between two sites (cluster-connectivity) is dependent on the inter-site distance, r. The connectivity, for example, is simply expressed by the jump rate of hopping carriers, $w(r)$, as follows [29, 30]:

$$w(r) = \begin{cases} (1 - r/r_0)^{\alpha} & \text{for } 0 \leqslant r \leqslant r_0 \\ 0 & \text{for } r > r_0 \end{cases} \tag{3}$$

where r_0 is the maximum distance of the carrier jump and α the fuzziness factor determining the connectivity. The ordinary percolation model corresponds to $\alpha = 0$, where the connectivity is constant within $r \leqslant r_0$. When $\alpha > 0$ the connectivity becomes weak and the carrier-jumping probability is strongly suppressed with increasing r. In this model, the μ value increases with α for $\alpha > 1$, owing to the wide distribution of the connectivity. Moreover, this model indicates that p_C is independent of α [30]. These arguments are consistent with the present results. Several theoretical results have also indicated that the wide distribution of connectivity plays an important role to yield the nonuniversal conductivity irrespective of metallic or hopping conduction systems [23–28, 31]. In the present Co-cluster-assembled system, such a wide distribution of connectivity against d will be attributable to the heterogeneous interface structures between Co clusters, i.e. lattice defects, imperfect contacts etc. These characters might be strongly affected by the cluster size because structural instability, such as structural fluctuation [33] and depression of melting point [34], is enhanced in small clusters when d is decreased. In order to understand the origins of the nonuniversal behaviours in the percolation of electrical conductivity in the present nanometre-sized Co-cluster assemblies, we are more precisely studying structure and connectivity of Co clusters through the high-resolution TEM observation.

5. Conclusion

We have randomly deposited monodispersed, nanometre-sized Co clusters on substrates using the PGC method. Based upon the measurement of TEM image and *in situ* electrical conductivity, we have elucidated how the deposited clusters on the substrate change from discontinuous to continuous networks. The percolation processes of Co clusters do not agree with the ordinary 2D percolation concept: they reveal nonuniversality in the scaling-law. The critical coverage of clusters (0.63) is much higher than the theoretical one (0.45), due mainly to the partial overlapping of deposited clusters, and also to an attractive interaction between the clusters. The critical exponent of the scaling-law increases with increasing the mean cluster diameter, d, although it is theoretically predicted to be independent of d. The anomalous features are interpreted by the soft-percolation model, which premises the distribution in the electrical connectivity between clusters. The critical thickness of the electrical percolation also depends on d, owing to the partial overlapping of deposited clusters. The geometrical percolation occurs slightly before the electrical one, being due to the limited range of TEM observation and the complex cluster interfaces.

Acknowledgments

This work was supported by Core Research for Evolutional Science and Technology (CREST) of Japan Science and Technology (JST) Corporation, and partly by a Grant-in-Aid for Scientific Research A1 (grant No 08505004). We appreciate Dr M Sakurai for his comment, Mr K Wakoh for his assistance during the present experiments and Professor T Odagaki for his comment. We were indebted to the support from the Laboratory for Developmental Research of Advanced Materials of our Institute.

References

[1] Edelstein A S and Cammarata R C (ed) 1996 *Nanomaterials: Synthesis, Properties and Applications* (Bristol: Institute of Physics)
[2] Hernando A (ed) 1993 *Nanomagnetism (NATO ASI Series E: Applied Science 247)* (Dordrecht: Kluwer)
[3] Haberland H (ed) 1994 *Clusters of Atoms and Molecules I and II* (Berlin: Springer)
[4] Melinon P, Paillard V, Dupuis V, Perez A, Jensen P, Hoareau A, Perez J P, Tuaillon J, Broyer M, Vialle J L, Pellarin M, Baguenard B and Lerme J 1995 *Int. J. Mod. Phys.* B **9** 339
[5] Yamamuro S, Sakurai M, Konno T J, Sumiyama K and Suzuki K 1998 *AIP Conf. Proc.* **416** 491
[6] Yamamuro S, Sumiyama K, Sakurai M and Suzuki K 1998 *Supramol. Sci.* **5** 239
[7] Yamamuro S, Sumiyama K and Suzuki K 1999 *J. Appl. Phys.* **85** 483
[8] Haberland H, Karrais M, Mall M and Thurner Y 1992 *J. Vac. Sci. Technol.* A **10** 3266
[9] Yamamuro S, Sumiyama K, Hihara T and Suzuki K *J. Phys. Soc. Japan* **68** 28
[10] Stauffer D and Aharony A 1992 *Introduction to Percolation Theory* (London: Taylor and Francis)
[11] Odagaki T 1993 *Science of Percolation* (Tokyo: Syokabo (in Japanese))
[12] Cheriet L, Helbig H H and Arajs S 1989 *Phys. Rev.* B **39** 9828
[13] Nan Ce-Wen 1993 *Prog. Mater. Sci.* **37** 1
[14] Yoshida K 1991 *Japan. J. Appl. Phys.* **30** 3482
[15] Fuchs G, Melinon P, Aires F S, Treilleux M, Cabaud B and Hoareau A 1991 *Phys. Rev.* B **44** 3926
[16] Melinon P, Jensen P, Hu J X, Hoareau A, Cabaud B, Treilleux M and Guillot D 1991 *Phys. Rev.* B **44** 12 562
[17] Yamamuro S, Sumiyama K and Suzuki K unpublished
[18] Scher H and Zallen R 1970 *J. Chem. Phys.* **53** 3759
[19] Shante V K S and Kirkpatrick S 1971 *Adv. Phys.* **20** 325
[20] Duckers L J and Ross R G 1978 *Phys. Lett.* A **49** 361
Duckers L J 1978 *Phys. Lett.* A **67** 93
[21] Harris A B 1983 *Phys. Rev.* B **28** 2614
[22] Octavio M, Gutierrez G and Aponte J 1987 *Phys. Rev.* B **36** 2461
[23] Kogut P M and Straley J P 1979 *J. Phys. C: Solid State Phys.* **12** 2151
[24] Ben-Mizrahi A and Bergman D J 1981 *J. Phys. C: Solid State Phys.* **14** 909
[25] Machta J, Guyer R A and More S M 1986 *Phys. Rev.* B **33** 4818
[26] Lubensky T C and Tremblay A-M S 1986 *Phys. Rev.* B **34** 3408
[27] Halperin B I, Feng S and Sen P N 1985 *Phys. Rev. Lett.* **54** 2391
[28] Feng S, Halperin B I and Sen P N 1987 *Phys. Rev.* B **35** 197
[29] Odagaki T 1989 *J. Phys.: Condens. Matter* **1** 1013
[30] Wachi Y, Odagaki T and Puri A 1994 *Phys. Rev.* B **50** 13 412
[31] Balberg I 1987 *Phys. Rev. Lett.* **59** 1305
[32] Wu J and McLachlan D S 1997 *Phys. Rev.* B **56** 1236
[33] Iijima S and Ichihashi T 1986 *Phys. Rev. Lett.* **56** 616
[34] Buffat Ph and Borel J-P 1976 *Phys. Rev.* A **13** 2287